

Multiuser Interference Mitigation in Non-coherent UWB Ranging via Nonlinear Filtering

Zafer Sahinoglu¹, Ismail Guvenc²

¹Mitsubishi Electric Research Labs, 201 Broadway Ave., Cambridge, MA, 02139

²Department of Electrical Engineering, University of South Florida, Tampa, FL, 33620

E-mail:{zafer, guvenc}@merl.com

Abstract—Ranging with energy detectors enables low-cost implementation. However, any interference can be quite detrimental to range accuracy. We develop a method that performs non-linear filtering on the received signal energy to mitigate multiuser interference (MUI); and we test it over time-hopping and direct sequence impulse radio ultrawideband signals. Simulations conducted over IEEE 802.15.4a residential line of sight ultrawideband multipath channels indicate that non-linear filtering helps sustain range estimation accuracy in the presence of strong MUI.

Index Terms—Ultrawideband, ranging, impulse radio, time of arrival, multi-user interference

I. INTRODUCTION

In time-of-arrival (ToA) based ranging, the range accuracy depends heavily on how well the ToA of a signal is estimated. Identifying multipath components and finding the leading path is crucial to decrease ranging errors. With its fractional bandwidth of 20%, or at least 500MHz bandwidth, an ultrawideband (UWB) signal provides high time resolution measured in nanoseconds; and it helps to separate individual multipath components better than narrowband signals [1].

In UWB ranging, tracking of the leading edge is challenging due to a vast number of multipaths and the fact that the line-of-sight (LoS) path may not have the highest amplitude. Traditionally, UWB approaches based on coherent reception require many rake fingers in order to combine energy from the received signal [2]. However, there is a strong desire to drive down UWB radio cost. This has led to an increased interest in alternative receiver techniques for UWB that do not require the hardware complexity of coherent rake receptions.

One intuitive approach has been a trade-off between high performance coherent receivers and low-complexity non-coherent receivers [3]. However, one of the major drawbacks of a non-coherent receiver is its performance in the presence of multiuser interference (MUI). In a multiuser network, signals from multiple devices may interfere with a desired signal and deteriorate the range error drastically. This is due to the fact that interference suppression techniques such as CDMA are not readily applicable to simple non-coherent receivers. Typically, processing gain is obtained by coherently combining received signal energy according to transmitted time-hopping or DS patterns [4]. However, in coherent energy combining, even a small amount of interference energy may be construed as a leading edge. Therefore, prior to coherent energy-combining, it is prudent to remove as much MUI energy as possible.

In this paper, our scope is to make ranging via non-coherent radios resilient to MUI. We focus on simple energy detectors, and propose a MUI mitigation technique for time-hopping impulse-radio (TH-IR) [5] and direct sequence impulse radio (DS-IR) UWB systems to sustain sub-meter range accuracy when MUI is present.

The remainder of this paper is organized as follows. In Section II, the literature on UWB ranging is reviewed. In Section III, the TH-IR and DS-IR UWB signal models are given and then the proposed receiver architecture is described. In Section IV, MUI mitigation via non-linear energy filtering is explained. Section V is allocated to the discussion of simulation results. Finally, the paper is concluded in Section VI with a summary of our future work.

II. TOA BASED UWB RANGING

Acquisition of a signal can be achieved by locking onto the strongest multipath component, which would result in a coarse ToA estimate [6]-[11]. However, precise ToA estimation requires identification of the leading path, which may not be the strongest. In [12], a generalized maximum likelihood (GML) approach is proposed to estimate the leading path by testing the paths prior to the strongest. A stopping rule is determined based on the statistics of the amplitude ratio and the delay between the strongest and the leading paths. However, very high sampling rates on the order of Nyquist rate is required. In [13], the authors relax the sampling rate requirements and propose a simpler threshold-based detection technique. In [14], the problem is approached as a break-point estimation for signal presence, where temporal correlation arising from the transmitted pulse is used to accurately partition the received signal.

Acquisition and ToA estimation can generally be achieved by using various transceiver types; e.g. matched filters (or stored-reference receivers), transmitted reference receivers, and energy detectors (ED) [6], [15]. The use of energy detectors for synchronization and ToA estimation in UWB systems has been investigated in [15], [16], [17]. ED receivers using threshold-based ToA estimation techniques are discussed in [18], [19], [20], a multi-scale product approach that improves the ranging accuracy was investigated in [21], and likelihood based techniques are proposed in [15]. A two-step hybrid ToA estimation via ED and matched filters are also studied in [22], [23], where the energy-detection step provides a coarse ToA estimate, and the matched-filtering step refines

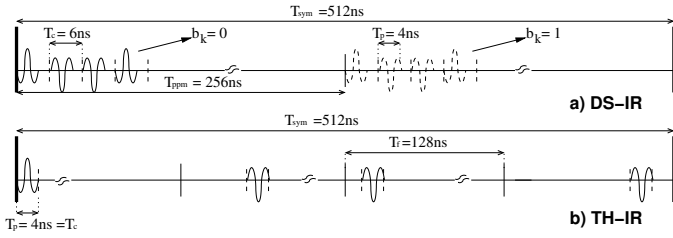


Fig. 1. Illustration of transmitted waveforms and simulation parameters for a) DS-IR, b) TH-IR.

the estimate. In [24], a matched-filter receiver's ability to differentiate between the desired user signal and interference for TH-IR UWB during synchronization is analyzed.

Our literature survey indicates that the ToA estimation problem for IR-UWB has been analyzed without consideration of MUI. Note that even though MUI mitigation is investigated extensively for IR-UWB systems for symbol detection [25]-[28], there is no reference that addresses interference mitigation for ToA estimation with non-coherent UWB radios to the best of our knowledge. This work is intended to fill this gap.

III. RANGING SIGNAL WAVEFORMS AND RECEIVER FRONT-END

In [19], four different waveforms were compared from the ranging perspective; In this work, we adopt two of them: DS-IR and TH-IR (see Fig.1). These are currently under consideration for standardization in the IEEE 802.15.4a Task Group.

Each IEEE 802.15.4a packet contains a preamble that consists of multiple repetition of a base symbol waveform; and the preamble is used for acquisition/synchronization and ranging. We adopt the IEEE 802.15.4a terminology and use the following notations in the sequel: $E_s^{(k)}$ denotes the symbol energy from the k th user, N_{sym} is the number of symbol repetition within the preamble, ω is the transmitted pulse shape with unit energy, T_{sym} is the symbol duration, T_p is the pulse duration, ϵ_k is the TOA of the k th user's signal and η is the zero-mean AWGN with variance $\sigma_n^2 = \frac{N_0}{2}$. L_k denotes the total number of multipath components for the k th user, $\gamma_{l,k}$ and $\tau_{l,k}$ represents the amplitude and delay of the l th multipath component for the k th user respectively, and N_s is the total number of pulses per symbol.

A receiver can process the preamble by either template matching (coherent) or energy detection (ED). Even though coherent ranging is superior, the ED receiver has its own advantages such as simplicity, operability at sub-Nyquist sampling rates (which determines the range resolution) and low cost. They are also more resilient to pulse shape distortion.

The ED receiver we study in this paper is illustrated in Fig. 2. It first feeds the received signal (after a band pass filter) into a square-law device, integrates its output, and then samples periodically. We denote these generated energy samples as $z[n]$, and the sampling interval and the number of samples per symbol as t_s and $n_b = \frac{T_{sym}}{t_s}$, respectively. The $z[n]$ are then regrouped into a 2D matrix.

Once a matrix is formed, it is passed through a non-linear filter to enhance desired signal energy parts and remove the

MUI. Afterwards, the matrix is converted back to 1D time series to locate the leading edge, by means of adaptive search-back and threshold techniques. In what follows, we present signal models for DS-IR and TH-IR systems.

A. DS-IR

In DS-IR, a symbol interval is divided into two halves. A group of closely spaced pulses called *burst* is transmitted either in the first or the second half in a pseudo-random pattern. With such an orthogonal burst positioning, ranging can be performed in the presence of multiple simultaneously operating devices. The received DS-IR symbol waveform from user k can be written as

$$\omega_{mp,k}^{(ds)}(t) = \sqrt{\frac{E_s^{(k)}}{N_s}} \sum_{l=1}^{L_k} \gamma_{l,k} \sum_{j=1}^{N_s} d_{j,k}^{(ds)} \times \omega\left(t - (j-1)T_c^{(ds)} - \tau_{l,k} - \epsilon_k\right), \quad (1)$$

where $d_{j,k}^{(ds)} \in \{\pm 1\}$ are the binary sequences for the k th user, and $T_c^{(ds)}$ is the chip duration (pulse repetition interval) such that $T_c^{(ds)} \geq T_p$. The polarities of the pulses in a burst are used to convey data for coherent reception. Therefore, the spacing between the pulses enables coherent receivers to demodulate the data.

If there are K simultaneously transmitting users, the received signal would be

$$r^{(ds)}(t) = \sum_{k=1}^K \sum_{\lambda=1}^{N_{sym}} \omega_{mp,k}^{(ds)}(t - \lambda T_{sym} - b_{\lambda,k} T_{ppm}) + \eta(t), \quad (2)$$

where $b_{\lambda,k} \in \{0, 1\}$ is the λ th symbol of k th user, T_{ppm} is the modulation index (i.e. delay) for pulse-burst position modulation (PPM). Note that varying T_{ppm} would change the inter-burst interval. Hence, multiple orthogonal waveforms can be generated, and each can be assigned to users of different networks.

The ED output samples at the desired receiver with the DS-IR waveforms is

$$z^{(ds)}[n] = \int_{(n-1)t_s}^{nt_s} |r^{(ds)}(t)|^2 dt, \quad (3)$$

where $n = 1, 2, \dots, N_b$, and $N_b = N_{sym} n_b$.

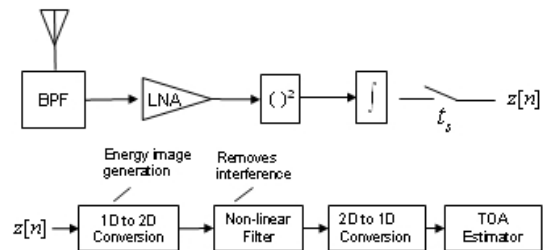


Fig. 2. Illustration of the energy imaging ranging receiver while processing ED outputs.

B. TH-IR

In TH-IR, a symbol is divided into virtual time intervals T_f called *frames*, which is further decomposed into smaller time slots $T_c^{(th)}$ called *chips*. A single pulse is transmitted in each frame on a chip location specified by a user specific pseudo-random time-hopping code. The received TH-IR signal from user k is

$$\omega_{mp,k}^{(th)}(t) = \sqrt{\frac{E_s^{(k)}}{N_s}} \sum_{l=1}^{L_k} \gamma_{l,k} \sum_{j=1}^{N_s} d_{j,k} \times \omega\left(t - (j-1)T_f - c_{j,k}T_c - \tau_{l,k} - \epsilon_k\right), \quad (4)$$

where $c_{j,k}$ and $d_{j,k}$ are the TH codes and polarity scrambling codes of user k , respectively. If K users are transmitting N_{sym} symbols simultaneously, each with a unique TH code, the received signal by the desired user becomes

$$r^{(th)}(t) = \sum_{k=1}^K \sum_{\lambda=1}^{N_{sym}} \omega_{mp,k}^{(th)}(t - \lambda T_{sym}) + \eta(t), \quad (5)$$

The collected energy samples at the ED receiver would be

$$z^{(th)}[n] = \int_{(n-1)t_s}^{nt_s} |r^{(th)}(t)|^2 dt. \quad (6)$$

C. Conventional Energy Combining (Conv)

A conventional receiver coherently combines the energies over N_{sym} symbols to improve the signal-to-noise ratio (SNR) using the bit sequence of the desired user in the DS-IR case¹, and over $N_{sym} \times N_s$ pulse positions using the TH sequences of the desired user in the TH-IR case. Then, a searchback algorithm is applied to locate the leading signal energy.

In this paper, we adopt the searchback scheme presented in [19]. With the assumption that the receiver is perfectly synchronized to the strongest energy sample, the algorithm tries to identify the leading edge by searching the samples backward within a predetermined window starting from the strongest sample. In non-LoS environments, the strongest path may arrive as much as 60ns after the first path [29]. At $4ns$ sampling period, this would correspond to 15 samples. Therefore, in the searchback algorithm (see Fig.3), it would be sufficient to have $W = 15$.

Each sample within the searchback window is compared to a threshold. Even if it is smaller than the threshold, the algorithm does not terminate; and it allows up to w_{cls} consecutive noise-only samples. This is because of the fact that clustering of the multipath components yields noise-only regions between the clusters. The threshold ξ that corresponds to a fixed P_{fa} is given by² [19]

$$\xi = \sigma_{ed} Q^{-1} \left(1 - (1 - P_{fa})^{\frac{1}{w_{cls}}} \right) + \mu_{ed}, \quad (7)$$

where μ_{ed} and σ_{ed} are the mean and the variance of noise-only samples. The optimal threshold is a function of w_{cls} .

¹For DS-IR, we assume that we do not combine energies from different pulses within the same symbol in order not to weaken the leading edge due to multipath effects [19].

²We define P_{fa} to be the probability of identifying a noise-only sample as a signal sample.

-
1. n_{max} : the index of the strongest energy sample,
 2. n_{le} := the index of the first signal energy sample,
 3. W : the searchback window length
 4. ξ := Noise based threshold,
 5. Let $i = n_{max}$, $w_{cls} = 2$,
 6. **while** $i \geq n_{max} - W$
 7. **if** $z[i] \geq \xi$ or $z[i-1] \geq \xi$ or $z[i-2] \geq \xi$
 8. $i = i - 1$,
 9. **else**
 10. **break**,
 11. **endif**
 12. **endwhile**
 13. Return $n_{le} = i + 1$.
-

Fig. 3. Pseudocode for the adaptive searchback algorithm to locate the leading signal energy

IV. ENERGY MATRIX FORMATION

SNR is one of the parameters that range estimation accuracy heavily depends on. Although the SNR can be improved via processing gain by coherently combining received signal energy samples [22], Fig.4 illustrates how poor the ranging performance would be after coherent energy combining in the presence of MUI. In the given TH-IR example, the symbol consists of four frames, and signal energy is integrated and sampled at a period such that it produces four samples in each frame and total 16 samples per symbol. The TH code of the desired signal is $\{0, 4, 4, 3\}$, and that of the interference is $\{0, 4, 5, 4\}$. Coherent combining requires energy samples $z[n]$ of the received signal to be combined in accordance with the matched TH code. In this example, it would produce the combined energy values $E[n]$ such that $E[n] = z[n+0] + z[n+4] + z[n+4+4] + z[n+4+4+3]$, where $0 \leq n \leq 3$, assuming that TOA ambiguity is as much as the frame duration. If there is no interference, $E[1] = 4A$ and $E[n] = 0$ for $n \neq 1$ and the TOA index is 1. In the presence of interference, the time of arrival information is very likely to be impacted, and it is easy to see in the example that TOA index becomes 0 because $E[0] = 2A$ (see Fig.4d).

We have now illustrated that signal design itself and coherent energy combining is not sufficient to deal with detrimental impact of interference. A solution simply lies in looking at the collected energy samples from a different view: two-dimensional energy matrix. Let us create a so-called energy matrix \mathbf{Z} of size $M \times N$, where M is the number of frames processed and N the number of energy samples collected from each frame. Referring to the previous example, the size of \mathbf{Z} would be 4×4 , it would be populated as

$$\mathbf{Z} = \begin{pmatrix} z[0+11] & z[1+11] & z[2+11] & z[3+11] \\ z[0+8] & z[1+8] & z[2+8] & z[3+8] \\ z[0+4] & z[1+4] & z[2+4] & z[3+4] \\ z[0+0] & z[1+0] & z[2+0] & z[3+0] \end{pmatrix} \quad (8)$$

Filling out each column of \mathbf{Z} with samples grouped according to the received signal's TH pattern would form vertical lines, whenever signal energy is present in all of those samples (Fig.4e). The detection of the left most vertical line would give the time index of the first arriving signal energy. If the interference follows a different TH pattern, intuitively the

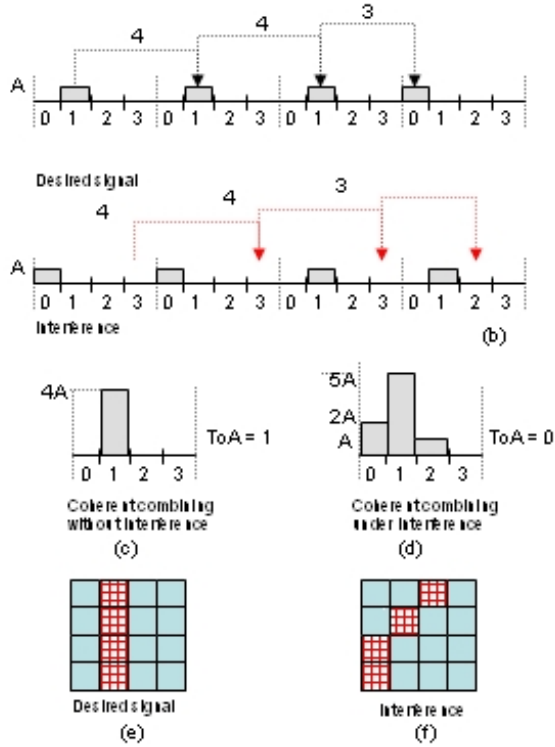


Fig. 4. Illustration of coherent energy combining in 1D a) Energy samples from TH-IR desired user, b) Energy samples from TH-IR interference c) Coherent combining of energy samples without interference d) Coherent combining of energy samples with interference e) Energy image of the desired signal, Z f) Energy image of the interference

energy matrix of the interference would not form a vertical line (Fig.4f).

The CONV does not account for the MUI and it directly aggregates the energy samples. This would be equivalent to summing the rows of \mathbf{Z} along each column, yielding an energy vector. Note that the column sum of the matrix in Fig.4e generates the energy vector in Fig.4c, and that of (e) + (f) results in Fig.4d.

Applying conventional leading edge detection techniques on the energy vector in Fig.4d would cause erroneous ranging due to interference. It is clear from the illustrations that the energy matrix would provide an insight into the presence and whereabouts of interference energy; and non-linear filters can be applied onto the matrix to mitigate this interference. The following subsections explain how to form an energy matrix from DS-IR and TH-IR waveforms.

A. Energy Matrix of DS-IR

Let λ denote the row index (which is also the symbol index), and κ denote the column index of the matrix. Then, the samples in (3) can be used to populate the matrix as follows

$$\mathbf{Z}^{(ds)}[\lambda, \kappa] = \mathbf{z}^{(ds)} \left[\kappa + (\lambda - 1)n_b + b_{\lambda,1} \frac{T_{ppm}}{t_s} \right]. \quad (9)$$

where $1 \leq \lambda \leq N_{sym}$ and $1 \leq \kappa \leq n_b$

A typical energy matrix of a DS-IR signal after passing through an IEEE 802.15.4a CM1 channel is given in Fig. 5 while the E_b/N_0 is 16dB for the desired received signal and

10dB for the interference. Clearly, the desired signal forms a vertical line indicating multi-path components, whereas the interference pattern is intermittent.

Self interference may be present too in the energy matrix. This happens when only some of the samples of a column do overlap with the energy from bursts.

The energy vector $\tilde{z}^{(ds)}$ that the *Conv* receiver generates would be equivalent to the column-sum of $\mathbf{Z}^{(ds)}$.

$$\tilde{z}^{(ds)} = \mathbf{1}_{N_{sym}} \mathbf{Z}^{(ds)}, \quad (10)$$

where $\mathbf{1}_{N_{sym}}$ is a column vector of all ones.

B. Energy Matrix of TH-IR

In TH-IR, energy samples given in eq.6 are grouped together according to the transmitted TH code, and samples of the same group are used to populate a column of the energy matrix $\mathbf{Z}^{(th)}$. As a result, there would be $N_s \times N_{sym}$ rows.

$$\mathbf{Z}^{(th)}[\lambda(j), \kappa] = \mathbf{z}^{(th)} \left[\kappa + (\lambda - 1)n_b + j \frac{T_f}{t_s} + c_{j,1} \frac{T_c}{t_s} \right], \quad (11)$$

where $\lambda(j) = N_s(\lambda - 1) + j$, and $j \in \{1, 2, \dots, N_s\}$. Note that we assume T_c to be an integer multiple of t_s in order to be able to collect the energies over integer number of pulses.

A typical energy matrix of a TH-IR signal after passing through an IEEE 802.15.4a CM1 channel is given in Fig.6. The E_b/N_0 is 16dB for the desired received signal and 10dB for the interference. Note that MUI and self-interference would cause short discrete lines. The actual ToA corresponds to the most left continuous vertical line in $\mathbf{Z}^{(th)}$.

A cause of the self-interference is the imperfect auto-correlation of the TH codes. Note that the energy samples of a column are grouped according to the desired user's TH code. It is possible that only some of the grouped samples would contain energy from the received signal due to a partial overlap with the signal's TH pattern. Especially, if the uncertainty region for the ToA is larger than T_f , the energy collection process would cause more self-interference. Non-linear filters would not be able to distinguish self-interference from MUI.

Furthermore, to suppress noise N_{img} matrices can be superseded, relying on the assumption that the statistics of interference and noise are stationary. The *Conv* would column-sum $\mathbf{Z}^{(th)}$ and would perform edge detection on $\tilde{z}^{(th)}$.

$$\tilde{z}^{(th)} = \mathbf{1}_{N_s N_{sym}} \mathbf{Z}^{(th)}. \quad (12)$$

V. NON-LINEAR MATRIX FILTERING

In this section, we consider two non-linear filters for interference mitigation: minimum filter and median filter. In the following discussion, without losing generality, we drop the superscript of the energy matrix for DS-IR and TH-IR, and refer to it as \mathbf{Z} .

A. Minimum Filter - Min

To remove outliers, which are most likely due to interference, in \mathbf{Z} , we apply length- W minimum filter along each column. The minimum filter replaces the center sample with

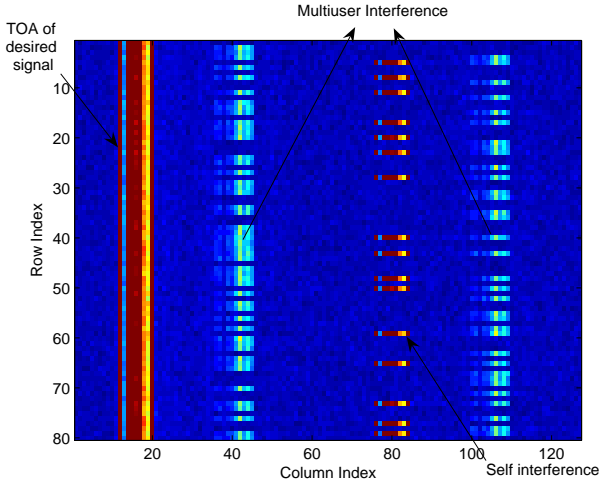


Fig. 5. Energy image for the DS-IR ($E_b^{(des)}/N_0 = 16\text{dB}$, $E_b^{(int)}/N_0 = 10\text{dB}$, $t_c = 4\text{ns}$, $N_s = 4$, $T_{sym} = 512\text{ns}$, $T_{ppm} = 256\text{ns}$, $n_b = 128$). The row index corresponds to symbols and the column index corresponds to the samples within a symbol interval

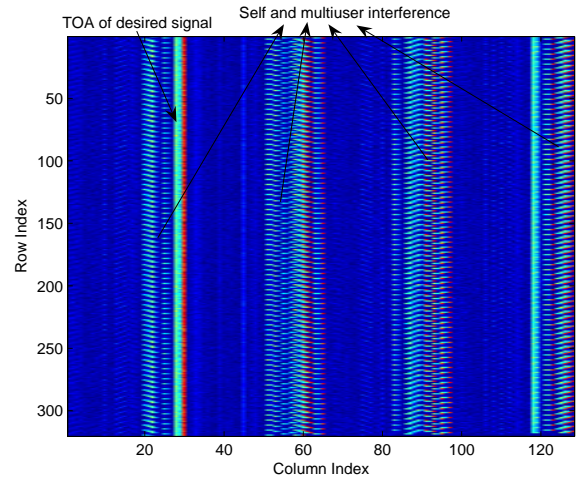


Fig. 6. Energy image for the TH-IR ($E_b^{(des)}/N_0 = 16\text{dB}$, $E_b^{(int)}/N_0 = 10\text{dB}$, $t_c = 4\text{ns}$, $N_s = 4$, $T_{sym} = 512\text{ns}$, $T_f = 128\text{ns}$, $n_b = 128$).

the minimum of the samples within the filter window. Then, the elements of the new energy matrix $\mathbf{Z}^{(min)}$ would be

$$\mathbf{Z}^{(min)}[\lambda, \kappa] = \min \left\{ \mathbf{Z}[\lambda, \kappa], \mathbf{Z}[\lambda + 1, \kappa], \dots, \mathbf{Z}[\lambda + W - 1, \kappa] \right\}, \quad (13)$$

where $\lambda \in \{1, 2, \dots, N_{sym} - W + 1\}$ for DS-IR and $\lambda \in \{1, 2, \dots, N_s N_{sym} - W + 1\}$ for TH-IR. Once the interference is removed, $\mathbf{Z}^{(min)}$ is converted to a vector by the column-sum operation,

$$\tilde{z}^{(ds, min)} = \mathbf{1}_{N_{sym} - W + 1} \mathbf{Z}^{(ds, min)}, \quad (14)$$

$$\tilde{z}^{(th, min)} = \mathbf{1}_{N_s N_{sym} - W + 1} \mathbf{Z}^{(th, min)}. \quad (15)$$

where $\mathbf{Z}^{(ds, min)}$ indicates *Min* filtered matrix for the DS-IR and $\mathbf{Z}^{(th, min)}$ for the TH-IR. Note that while it significantly removes the interference, The *Min* filter may also degrade the desired signal.

B. Median Filter - Median

One well-known non-linear filter is the median filter. Median filters are special cases of stack filters and they have been widely used in digital image and signal processing [30], [31] to remove singularities caused by noise. A median filter replaces the center value in a given data set with the median of the set. A longer filter length makes output noise more colored and becomes less effective to mitigate interference, because any unsuppressed interference energy may propagate onto its neighboring samples. We use length-3 median filter in the simulations and refer to it as *Median*. One way to prevent output noise from being colored is to apply the median-filter in non-overlapping windows. In appendix A, we quantify the impact of non-overlapping median filtering on detection performance of DC signals in white Gaussian noise to provide

some insight into more complex detection problems. In (16), $\mathbf{Z}^{(med)}$ is the energy matrix at the output of the median filter.

$$\mathbf{Z}^{(med)}[\lambda, \kappa] = \text{median} \left\{ \mathbf{Z}[\lambda, \kappa], \mathbf{Z}[\lambda + 1, \kappa], \dots, \mathbf{Z}[\lambda + W - 1, \kappa] \right\}, \quad (16)$$

After converting $\mathbf{Z}^{(med)}$ into an energy vector, we have

$$\tilde{z}^{(ds, med)} = \mathbf{1}_{N_{sym} - W + 1} \mathbf{Z}^{(ds, med)}, \quad (17)$$

$$\tilde{z}^{(th, med)} = \mathbf{1}_{N_s N_{sym} - W + 1} \mathbf{Z}^{(th, med)}. \quad (18)$$

The leading edge search is performed on $\tilde{z}^{(ds, med)}$ for DS-IR waveforms and on $\tilde{z}^{(th, med)}$ for TH-IR waveforms.

Note that both minimum and median filtering add to the low complexity of an energy-detection receiver. Assume that $z[n]$ are provided by a 16-bit ADC. Then, the memory requirement for storing \mathbf{Z} of size $M \times N$ would be $2MN$ Bytes. It is known that sorting W numerals has an inherent computational complexity of $O(W \log W)$. Thus, the overall complexity of applying *Median* or *Min* would be $M(N - W + 1)O(W \log W)$.

VI. SIMULATION RESULTS

The DS-IR and TH-IR signals are transmitted over IEEE 802.15.4a CM1 (residential line-of-sight) channels. For performance comparison, we use mean absolute error (MAE) of ToA estimations over 1000 realizations. A DS-IR or TH-IR symbol waveforms of length 512ns are considered; the other simulation settings are as follows: $T_{sym} = 512\text{ns}$, $T_{ppm} = 256\text{ns}$, $T_f = 128\text{ns}$, $T_p = 4\text{ns}$, $w_{cls} = 2$, $T_c = 4\text{ns}$ for TH-IR and 6ns for DS-IR, and the integration interval is 4ns. Energy images are obtained using 80 symbols (therefore yielding 80 rows for DS-IR, and 320 rows for TH-IR), and the images are further assumed to be averaged over 250 realizations³. For TH-IR, the time hopping sequence for the

³We assume that the bit sequences used in DS-IR repeat at every 80 symbols; the total preamble length considered for ranging purposes is therefore $512 \times 80 \times 250 \approx 10\text{ms}$.

desired user is $c_{j,1} = [1, 1, 4, 2]$, and for the interfering user $c_{j,2} = [1, 4, 2, 1]$, where there are $T_f/T_c = 64$ chip positions per frame⁴.

We compare the ranging accuracy of the searchback algorithm described in Fig. 3 under different interference levels. Let $E^{(1)}$ and $E^{(2)}$ denote the symbol energies received from the desired user and the interfering user, respectively (we also use E_b for desired user's bit energy). Then, we simulate the interference levels where $E^{(2)}/N_0 \in \{-\infty, 0, 5, 10\}$ dB. Energy matrices are constructed, and MAEs before (*Conv*) and after non-linear filtering (*Min*, *Median*) are obtained for all cases using a non-linear filter window length of 3.

A. DS-IR

The MAE results in Fig.8a) show that in the absence of MUI, the *Conv* and *Median* outperforms *Min* by achieving MAE of as low as $2ns$ at E_b/N_0 values less than 14dB. Intuitively, this is because of the fact that when noise is the dominant term, the *Min* penalizes the signal.

However, at higher E_b/N_0 , the MAE of the *Min* is better than those of both *Conv* and *Median*, because at high E_b/N_0 , self interference becomes the dominant factor, and (for certain channel realizations) the multipath components from a previous symbol may extend into the searchback window and still degrade the ranging accuracy of *Conv* and *Median* (see Fig. 5). Minimum filter remains effective to mitigate self interference at high SNRs.

The MAEs of the three approaches at $E^{(2)}/N_0 \in \{0, 5, 10\}$ dB are presented in Fig.8b), Fig.9a), and Fig.9b), respectively. The MAE error floors of the *Conv* and *Median* are approximately 5ns, 7ns and 9ns at interference levels of 0dB, 5dB and 10dB respectively. Whereas, the *Min* provides a much smaller error floor. When $E^{(2)}/N_0 = 0dB$ and $E^{(1)}/N_0$ is higher than 9dB, the *Min* can achieve the MAE of 3ns (sub-meter range accuracy). The *Min* requires at least $E^{(1)}/N_0 = 10dB$ at $E^{(2)}/N_0 = 5dB$ to keep the MAE below 3ns, and $E^{(1)}/N_0 = 16dB$ at $E^{(2)}/N_0 = 10dB$.

B. TH-IR

In general, the TH-IR waveform yields higher MAEs when compared to the DS-IR for the simulated set of parameters. This can be explained by higher self interference from autocorrelation sidelobes of TH-IR waveforms; even though TH sequences with a large zero correlation zones are used in our simulations, for the channels with large maximum excess delays, the performance is degraded. In the DS-IR case, the *Min* effectively suppressed self interference even at high E_b/N_0 .

An interesting observation with TH-IR waveforms is that there exists an optimum E_b/N_0 and the MAE starts increasing beyond this value even if there is no MUI. This is due to the fact that increasing the E_b/N_0 also increases the energy of autocorrelation sidelobes; since threshold is set based only on the noise level, stronger self interference starts degrading the performance after the optimum SNR level⁵.

⁴These sequences are obtained using a brute-force computer search so that they have a zero correlation zone larger than 100ns.

⁵The searchback algorithm in Fig. 3 continues to iterate due to multipath interference rather than terminating at the leading edge.

In the presence of interference, the MAEs of the three approaches at $E^{(2)}/N_0 \in \{0, 5, 10\}$ dB are presented in Fig.10b), Fig.11a), and Fig.11b), respectively.

The presence of interference at levels of $E^{(2)}/N_0 = 0dB$ or higher drastically hits the performance of *Conv* and *Median* and as a result their MAE never goes below 6ns; whereas the MAE of *Min* remains the same as no interference case when $E^{(2)}/N_0 = \{0, 5\}$ dB. Even when $E^{(2)}/N_0 = 10dB$, the MAE floor of the *Min* approaches 5ns at very high SNR ($E^{(1)}/N_0 = 18dB$).

These results suggest that a better search-back and thresholding techniques need to be developed for the TH-IR case for more accurate ranging performance. Also, the energy matrix with minimum filtering proves to be effective to deal with interference in TH-IR case too.

VII. CONCLUSION

In this paper, we introduce a ranging method that uses a matrix of received energy samples from a square-law device, and applies non-linear filtering on the matrix to remove the outliers caused by interference. The recommended non-linear filter, based on the simulation results, is the minimum filter. After the non-linear filtering, energy values along each column of the matrix are aggregated. Hence, the two dimensional data are converted into an energy vector. Then, a search-back algorithm is run on the energy vector to locate the leading signal energy.

The effectiveness of this approach is proven by simulations conducted using IEEE 802.15.4a channel models. Non-linear filtering changes noise and signal characteristics. Due to space limitations, the impact of non-linear filtering on the receiver detection performance will be studied in a different article.

This study reveals the following:

- Ranging is quite sensitive to interference, since the leading edge sample may be very weak compared to interference samples.
- A single interference energy sample may prolong the searchback process, and increase ranging error.
- In addition to multiuser interference, the searchback algorithm has to deal with self interference.

All in all, the paper presents a framework and provides practical algorithms to deal with multiuser interference in TOA estimation via non-coherent ultrawideband systems. Our future work includes development of adaptive algorithms (e.g. minimum and median filters with adaptive window size) for enhanced ranging accuracy under varying levels of interference, and quantification of the impact of non-linear filtering on detection performance.

ACKNOWLEDGMENTS

The authors wish to thank Dr. Philip Orlik and Dr. Andy F. Molisch for their fruitful feedback and comments during the course of this work; and they are also thankful to anonymous reviewers for their help to improve this presentation.

APPENDIX

Consider a problem of detecting a DC level in a known Gaussian noise, and assume that the noise distribution has

zero mean and variance σ^2 . Assume that there are N i.i.d. observations of the test data $z[n]$. When there is no signal, the data set belongs to a noise only hypothesis H_0 , and when signal is present it belongs to hypothesis H_1 .

$$\begin{aligned} H_0 : \mathbf{z}[n] &= w[n] & n &= 1, 2, \dots, N \\ H_1 : \mathbf{z}[n] &= A + w[n] & n &= 1, 2, \dots, N \end{aligned} \quad (19)$$

The probability of detection, P_D , with the Neyman-Pearson detector for this problem is given in [32] as

$$P_D = Q\left(Q^{-1}(P_{FA}) - \sqrt{\frac{NA^2}{\sigma_n^2}}\right) \quad (20)$$

Note that After length- W median filtering with non-overlapping windows, the new observation set would have only N/W samples and the noise variance would be scaled by $f(W)$, where $f(\cdot)$ indicates the function of. Since the input distribution is Gaussian, the output would approximate to Gaussian with the same mean, but lower variance [33].

Theoretically, the output density of the length 3 median filter is

$$p_2(y) = 6Q_z(y)(1 - Q_z(y))p_z(y) \quad (21)$$

where Q_z is the complementary cumulative distribution function and $p_z(y)$ is the density of the input data. Our numerical analysis indicates that $f(3) = 0.44$, and it provides a tight approximation to (21). The Kolmogorov-Smirnov test to compare the approximated density function and (21) results in the significance level of 0.1%. Then, in consideration of the approximation, the probability of detection P_D^m after median filtering becomes

$$P_D^m = Q\left(Q^{-1}(P_{FA}) - \sqrt{\frac{(N/W)A^2}{f(W) \times \sigma_n^2}}\right) \quad (22)$$

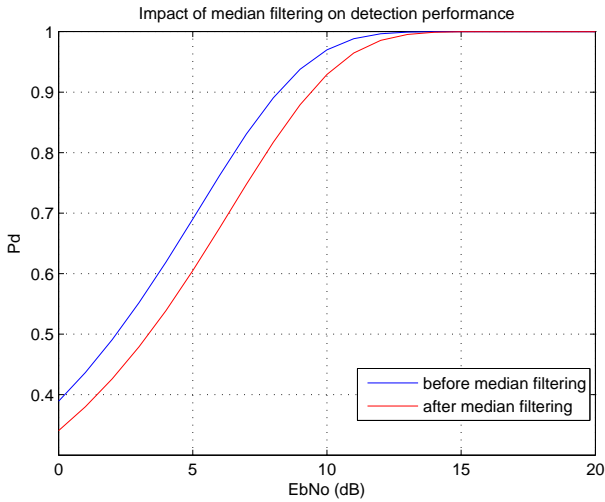


Fig. 7. Degradation in probability of detection after length-3 median filtering for "DC level detection in Gaussian noise" problem. Note that $W = 3$, $f(3) = 0.44$. Note that median filtering with non-overlapping windows degrades detection performance.

Here the problem of detecting a DC level in Gaussian noise is addressed for its simplicity, and in Fig.7 it is shown that median filtering in non-overlapping windows would lower the

probability of detection. If the length-3 median filter is applied with two-sample overlapping windows, the output noise would be a colored Gaussian, but the size of the observation set would remain as N . It may be possible to observe an increase in detection performance. Quantification of the impacts of median filtering with overlapping windows on the detection performance of non-coherent receivers will be studied in detail in another study.

REFERENCES

- [1] Z. Tarique, W. Q. Malik, and D. J. Edwards, "Bandwidth requirements for accurate detection of direct path in multipath environment," *IEE Electron. Lett.*, vol. 42, no. 2, pp. 100–101, Jan. 2006.
- [2] M. Z. Win, G. Chrisikos, and N. Sollenberger, "Performance of rake reception in dense multipath channels: Implications of spreading bandwidth and selection diversity order," *IEEE J. Select. Areas Commun.*, vol. 18, no. 8, pp. 1516–1525, August 2000.
- [3] J. Ellis and et. al., "IEEE P802.15.4a WPAN alternate PHY - PAR," Jan., 2004, doc.: IEEE 802.15-04/048r1. [Online]. Available: <http://www.ieee802.org/15/pub/TG4a.html>
- [4] S. Gezici, Z. Tian, G. B. Giannakis, H. Kobayashi, A. F. Molisch, H. V. Poor, and Z. Sahinoglu, "Localization via UWB radios," vol. 22, no. 4, pp. 70–84, July 2005.
- [5] M. Z. Win and R. A. Scholtz, "Impulse radio: How it works," *IEEE Comm. Letters*, vol. 2, no. 2, Feb 1998.
- [6] L. Reggiani and G. M. Maggio, "Rapid search algorithms for code acquisition in UWB impulse radio communications," *IEEE J. Select. Areas Commun.*, vol. 23, no. 5, pp. 898–908, May 2005.
- [7] J. Yu and Y. Yao, "Detection performance of time-hopping ultrawideband LPI waveforms," in *Proc. IEEE Sarnoff Symp.*, Princeton, New Jersey, Apr. 2005.
- [8] Z. Tian and G. B. Giannakis, "A GLRT approach to data-aided timing acquisition in UWB radios – Part I: Algorithms," *IEEE Trans. Wireless Commun.*, vol. 4, no. 6, pp. 2956–2967, Nov. 2005.
- [9] Z. Tian and G. B. Giannakis, "A GLRT approach to data-aided timing acquisition in UWB radios – Part II: Training sequence design," *IEEE Trans. Wireless Commun.*, vol. 4, no. 6, pp. 2994–3004, Nov. 2005.
- [10] W. Chung and D. Ha, "An accurate ultra wideband (UWB) ranging for precision asset location," in *Proc. IEEE Conf. Ultrawideband Syst. Technol. (UWBST)*, Reston, VA, Nov. 2003, pp. 389–393.
- [11] R. Fleming, C. Kushner, G. Roberts, and U. Nandiwada, "Rapid acquisition for ultra-wideband localizers," in *Proc. IEEE Conf. Ultrawideband Syst. Technol. (UWBST)*, Baltimore, MD, May 2002, pp. 245–249.
- [12] J.-Y. Lee and R. A. Scholtz, "Ranging in a dense multipath environment using an UWB radio link," *IEEE J. Select. Areas Commun.*, vol. 20, no. 9, pp. 1677–1683, Dec. 2002.
- [13] R. A. Scholtz and J. Y. Lee, "Problems in modeling UWB channels," in *Proc. IEEE Asilomar Conf. Signals, Syst. Computers*, vol. 1, Monterey, CA, Nov. 2002, pp. 706–711.
- [14] C. Mazzucco, U. Spagnolini, and G. Mulas, "A ranging technique for UWB indoor channel based on power delay profile analysis," in *Proc. IEEE Vehic. Technol. Conf. (VTC)*, Los Angeles, CA, Sep. 2004, pp. 2595–2599.
- [15] I. Guvenc and Z. Sahinoglu, "TOA estimation with different IR-UWB transceiver types," in *Proc. IEEE Int. Conf. UWB (ICU)*, Zurich, Switzerland, Sept. 2005, pp. 426–431.
- [16] A. Rabbachin and I. Oppermann, "Synchronization analysis for UWB systems with a low-complexity energy collection receiver," in *Proc. IEEE Conf. Ultrawideband Syst. Technol. (UWBST)*, Kyoto, Japan, May 2004, pp. 288–292.
- [17] K. Yu and I. Oppermann, "Performance of UWB position estimation based on time-of-arrival measurements," in *Proc. IEEE Conf. Ultrawideband Syst. Technol. (UWBST)*, Kyoto, Japan, May 2004, pp. 400–404.
- [18] I. Guvenc and Z. Sahinoglu, "Threshold-based TOA estimation for impulse radio UWB systems," in *Proc. IEEE Int. Conf. UWB (ICU)*, Zurich, Switzerland, Sept. 2005, pp. 420–425.
- [19] I. Guvenc, Z. Sahinoglu, A. F. Molisch, and P. Orlik, "Non-coherent TOA estimation in IR-UWB systems with different signal waveforms," in *Proc. IEEE Int. Workshop on Ultrawideband Networks (UWBNETS)*, Boston, MA, July 2005, pp. 245–251, (invited paper).
- [20] I. Guvenc and Z. Sahinoglu, "Threshold selection for UWB TOA estimation based on kurtosis analysis," *IEEE Commun. Lett.*, vol. 9, no. 12, pp. 1025–1027, Dec. 2005.
- [21] I. Guvenc and Z. Sahinoglu, "Multiscale energy products for TOA estimation in IR-UWB systems," in *Proc. IEEE Global Telecommun. Conf. (GLOBECOM)*, vol. 1, St. Louis, MO, Dec. 2005, pp. 209–213.

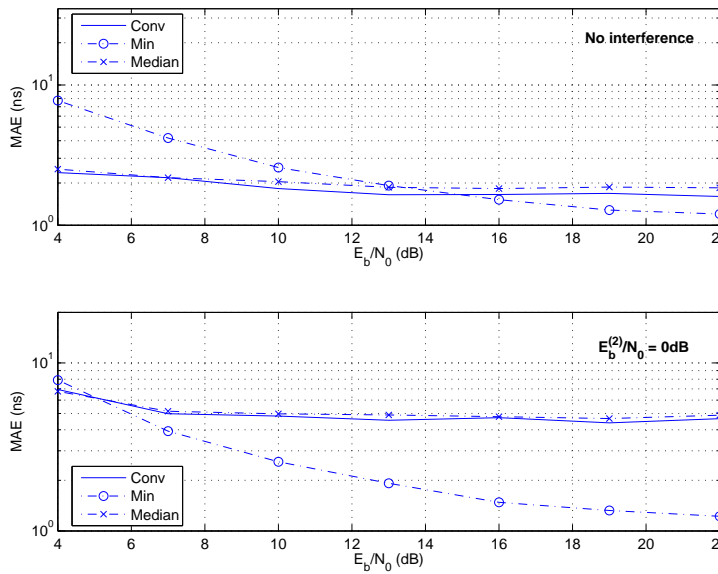


Fig. 8. MAEs for DS-IR: a) no interference, and b) $E_b^{(2)}/N_0 = 0\text{dB}$ ($w_{cls} = 2$)

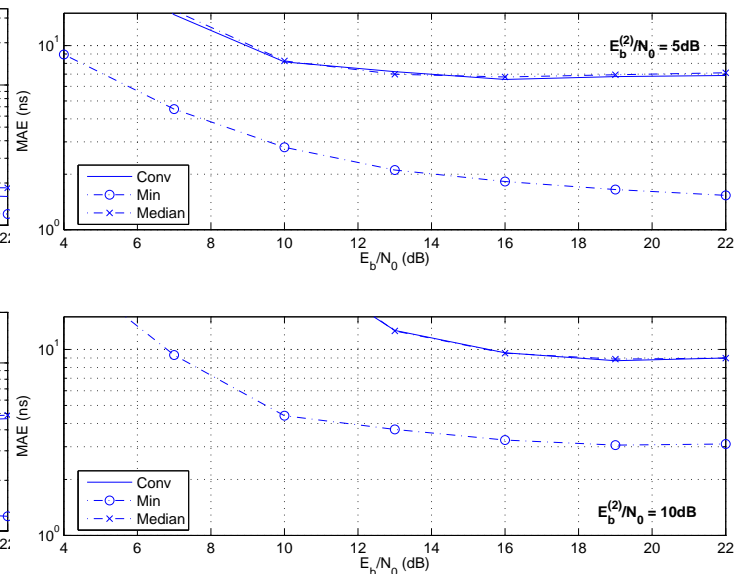


Fig. 9. MAEs for DS-IR: a) $E_b^{(2)}/N_0 = 5\text{dB}$, and b) $E_b^{(2)}/N_0 = 10\text{dB}$ ($w_{cls} = 2$)

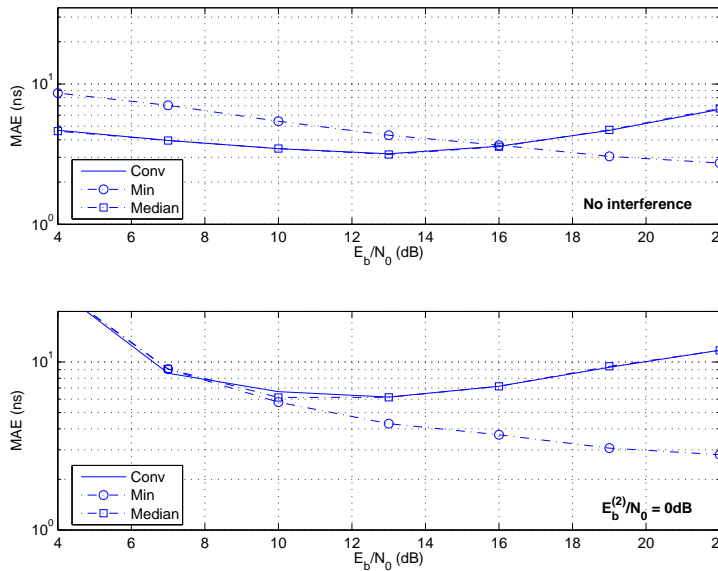


Fig. 10. MAEs for TH-IR: a) no interference, and b) $E_b^{(2)}/N_0 = 0\text{dB}$ ($w_{cls} = 2$)

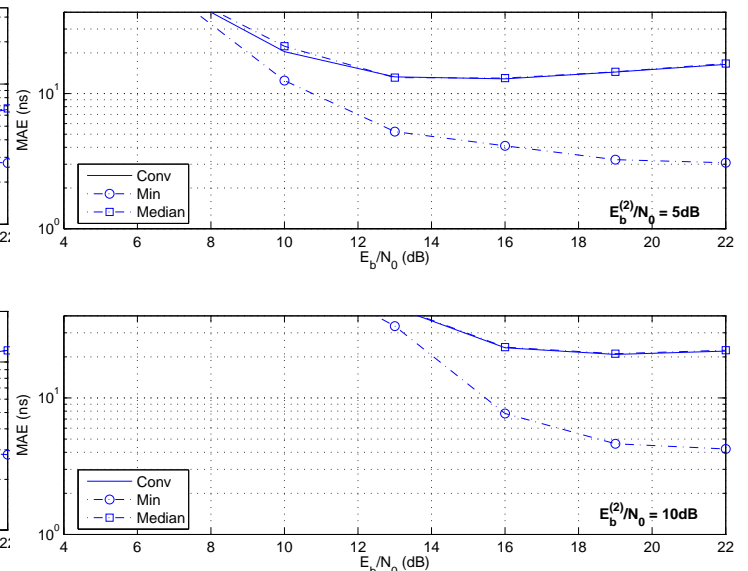


Fig. 11. MAEs for TH-IR: a) $E_b^{(2)}/N_0 = 5\text{dB}$, and b) $E_b^{(2)}/N_0 = 10\text{dB}$ ($w_{cls} = 2$)

- [22] S. Gezici, Z. Sahinoglu, H. Kobayashi, H. V. Poor, and A. F. Molisch, "A two-step time of arrival estimation algorithm for impulse radio ultrawideband systems," in *Proc. 13th European Signal Processing Conf. (EUSIPCO)*, Antalya, Turkey, Sep. 2005.
- [23] S. Gezici, Z. Sahinoglu, H. Kobayashi, and H. V. Poor, *Ultra Wideband Geolocation*. John Wiley & Sons, Inc., 2005, in *Ultrawideband Wireless Communications*.
- [24] R. Merz, C. Botteron, and P. A. Farine, "Multiuser interference during synchronization phase in UWB impulse radio," in *Proc. IEEE Int. Conf. UWB (ICU)*, Zurich, Switzerland, Sept. 2005, pp. 661–666.
- [25] S. Gezici, H. Kobayashi, and H. V. Poor, "A comparative study of pulse combining schemes for impulse radio UWB systems," in *Proc. IEEE Sarnoff Symp.*, Princeton, NJ, Apr. 2004, pp. 7–10.
- [26] S. Gezici, H. Kobayashi, H. V. Poor, and A. F. Molisch, "Optimal and suboptimal linear receivers for time-hopping impulse radio systems," in *Proc. IEEE Ultrawideband Systems and Technol. (UWBST)*, Kyoto, Japan, May 2004, pp. 11–15.
- [27] W. M. Lovelace and J. K. Townsend, "Chip discrimination for large near-far power ratios in UWB networks," in *Proc. IEEE Military Commun. Conf. (MILCOM)*, vol. 2, Oct. 2003, pp. 868–873.
- [28] E. Fishler and H. V. Poor, "Low complexity multi-user detectors for time hopping impulse radio systems," *IEEE Trans. Sig. Processing*, vol. 52, no. 9, pp. 2561–2571, Sept. 2004.
- [29] A. F. Molisch and et. al., "IEEE 802.15.4a channel model - final report," 2005, tech. rep. doc: IEEE 802.15-04-0662-02-004a. [Online]. Available: <http://www.ieee802.org/15/pub/TG4a.html>
- [30] H. G. Senel, R. A. Peters, and B. Dawant, "Topological median filters," *IEEE Trans. Image Proc.*, vol. 11, no. 2, pp. 89–104, Feb 2002.
- [31] N. C. Gallagher and G. L. Wise, "A theoretical analysis of the properties of median filters," *IEEE Trans. Acous. Speech Signal Proc.*, vol. 29, no. 6, pp. 1136–1141, Dec 1981.
- [32] S. M. Kay, *Fundamentals of Statistical Signal Processing: Detection Theory*. Upper Saddle River, NJ: Prentice Hall, Inc., 1998.
- [33] L. Yin, R. Yang, M. Gabbouj, and Y. Neuvo, "Weighted median filters: A tutorial," *IEEE Trans. Circuits and Systems - II: Analog and Digital Signal Processing*, vol. 43, no. 3, pp. 157–192, March 1996.